Co-precipitation vs. Green Synthesis: A Comparative Analysis of Structure, Morphology, Optical Properties, and Antibacterial Activity of Ag/ZnO Nanocomposite

ABSTRACT

Ag/ZnO nanocomposites were successfully prepared through co-precipitation (CS) and a green synthesis (GS) route mediated by Moringa Oleifera. The confirmation of their formation was evident from the simultaneous presence of Ag and ZnO reflections in powder X-ray diffraction. Field emission scanning electron microscopy (FESEM) analysis disclosed an average particle size of approximately 22 nm and 146 nm for CS and GS samples, respectively. The CS sample exhibited a distinctive flower-like morphology, indicating a unique self-assembly and growth pattern, while the GS sample displayed an almost rectangular shape. Structural composition and functional groups in the nanocomposites were analyzed using FT-IR spectroscopy. The direct band gaps were determined as 3.12 eV for CS and 3.10 eV for GS samples using a Tauc plot derived from UV-Vis NIR spectrometry. Notably, the antibacterial evaluation of the green-synthesized Ag/ZnO exhibited a pronounced zone of inhibition against both gram-positive (S. aureus) and gram-negative (E. coli) bacteria, demonstrating superior efficacy compared to chemically prepared Ag/ZnO. Overall, the study highlights the successful synthesis, structural characterization, and enhanced antibacterial properties of Ag/ZnO nanocomposites via a green route mediated by Moringa Oleifera.

Keywords: Ag/ZnO; Nanocomposite; Green Synthesis; Moringa Oleifera; Anti-bacterial Activity

1. INTRODUCTION

Over the last decade, significant strides have been made in the synthesis of noble metal nanoparticles using plant-mediated extracts, driven by their diverse applications [1]. Ahmed et al. investigated the production of antimicrobial silver (Ag) nanoparticles utilizing Azadirachta indica leaves extract, showing promise for biomedical applications [2]. Alex and collaborators employed leaves from different plants, including neem, aloe Vera, Indian mint, and guava, to synthesize silver nanoparticles (Ag NPs). Notably, Ag NPs synthesized with neem leaf extract exhibited a distinctive surface plasmon resonance (SPR) band and demonstrated bio-sensing properties, exemplified in the assessment involving Mancozeb fungicide [3]. Zinc oxide (ZnO), known for its diverse nanostructures and unique properties, has been extensively studied for various applications, such as nano-electronic/nano-optical devices, energy storage, cosmetics, and nano-sensors [4-9]. Characterized as a wide band gap semiconductor (3.37 eV) with a high exciton binding energy (60meV), ZnO displays efficient blue and near-UV excitonic emission [10]. Its low toxicity, biodegradability, and FDA approval for use in sunscreens underscore its appeal for biomedical applications. The ability of ZnO to dissolve under specific conditions, such as in acidic tumor environments, further enhances its potential in biomedical applications. ZnO nanomaterials have gained attention for their low toxicity, biodegradability, and favourable interactions with biological systems, making them attractive for biomedical applications [11, 12]. The dissolution of ZnO under certain conditions, such as in acidic environments or strong basic conditions, adds to its versatility [13].

Metal and metal oxide nanoparticles, especially Ag/ZnO nanocomposites, have emerged as potent antibacterial agents due to their high reactivity stemming from a remarkable surface area-to-volume ratio [14, 15]. These nanocomposites hold potential for applications in environmental health, particularly in developing antimicrobial compounds for water disinfection, showcasing superior efficacy compared to pure ZnO nanoparticles. Despite various synthesis techniques for Ag/ZnO nanocomposites, such as co-precipitation, sol–gel,

and hydrothermal synthesis, facing challenges like high temperatures, extended reaction times, and chemical waste generation, there is a growing demand for environmentally friendly synthesis methods [16-18]. In the realm of green synthesis, nanomaterial characteristics are shaped by the unique concentration and combination of biomolecules present in each plant extract [19]. This diversity encourages further exploration of different plant species for nanomaterial synthesis, emphasizing the need for environmentally friendly technologies in large-scale production. The rationale behind utilizing Ag/ZnO nanocomposites in research lies in their synergistic combination of unique properties. Silver nanoparticles bring potent antibacterial attributes, while ZnO contributes excellent photocatalytic and electronic features. The integration of these materials results in nanocomposites with enhanced antibacterial efficacy, catalytic activity, and tunable electrical and optical properties [11, 12]. Such versatile characteristics make Ag/ZnO nanocomposites appealing for applications spanning from biomedical uses, such as wound healing and drug delivery, to environmental remediation and optoelectronic devices. The ability to tailor their properties through controlled synthesis adds further appeal, positioning Ag/ZnO nanocomposites as promising materials for addressing multifaceted scientific and technological challenges.

The current work presents a comparative analysis of synthesizing an Ag/ZnO nanocomposite using both co-precipitation and a green synthesis method mediated by Moringa Oleifera. Moringa oleifera plant components have been documented to contain a diverse array of phytochemical constituents [20]. This plant serves as a notable reservoir of antioxidants, featuring compounds like quercetin and chlorogenic acids. Additionally, it is rich in various beneficial elements, encompassing flavonoids, phenolic, astragalin, anthocyanin, cinnamates, and carotenoids. Moringa oleifera is recognized for its substantial content of essential nutrients, including carotene, iron (Fe), potassium (K), calcium (Ca), as well as terpenes, quinines, saponins, alkaloids, proteins, tannins, and vitamin C [21, 22]. The objective is to explore the

impact of Moringa Oleifera on the structural, morphological, optical, and antibacterial properties through various characterization techniques, including X-Ray Diffraction (XRD), Field-Emission Scanning Electron Microscopy (FESEM), Fourier Transform Infrared Spectroscopy (FTIR), UV-Vis Spectroscopy, and Antibacterial Assay.

2. MATERIAL AND METHODS

2. 1. Co-Precipitation Method

Zinc di-nitrate hexahydrate (ZnO $(NO_3)_2 \cdot 6H_2O$) at a quantity of 0.4mol was dissolved in a mixture of 40 mL ethanol and 10 mL water, stirred for 2 hours. Subsequently, a solution containing silver nitrate ($AgNO_3$) at 0.045mol and 10 mL of NaOH was added dropwise, followed by the gradual addition of $NaBH_4$ (0.5 mg) dissolved in 5 mL ice-cold water. Throughout this procedure, the precipitate underwent a colour transformation from colourless to brownish, indicating the formation of the nanocomposite. The resultant product was collected through centrifugation at 6000 rpm for 1 hour, underwent several washes with distilled water and ethanol, and was then dried at 100°C for 24 hours, resulting in the formation of the Ag/ZnO nanocomposite.

2. 2. Green Synthesis

Schematic representation of Ag/ZnO biosynthesis using Moringa leaf extract and characterization techniques is given in Fig. 1**.** Dust-free and disease-free Moringa Oleifera leaves were thoroughly washed with deionized water and air-dried at room temperature for 24 hours. Subsequently, 30 g of the dried leaves were boiled in 200 mL of water at 100^{o}C for 30 minutes. The resulting green extract was filtered through Whatman No. 1 filter paper and stored in a refrigerator for future use. Next, 40 mL of the Moringa Oleifera leaves extract was mixed with 40 mL of ethanol at room temperature and stirred for 30 minutes. Zinc di-nitrate hexahydrate was then added to the Moringa Oleifera leaf extract with continuous stirring at 100^{o}C until a creamy solid product formed. Following this, $AgNO_3$ was mixed with deionized

water and added dropwise to the suspension, continuing the stirring process for 1 hour. The final product was washed with deionized water, followed by ethanol, and dried in a hot air oven at 100^{o}C for 24 hours, resulting in the green-synthesized Ag/ZnO.

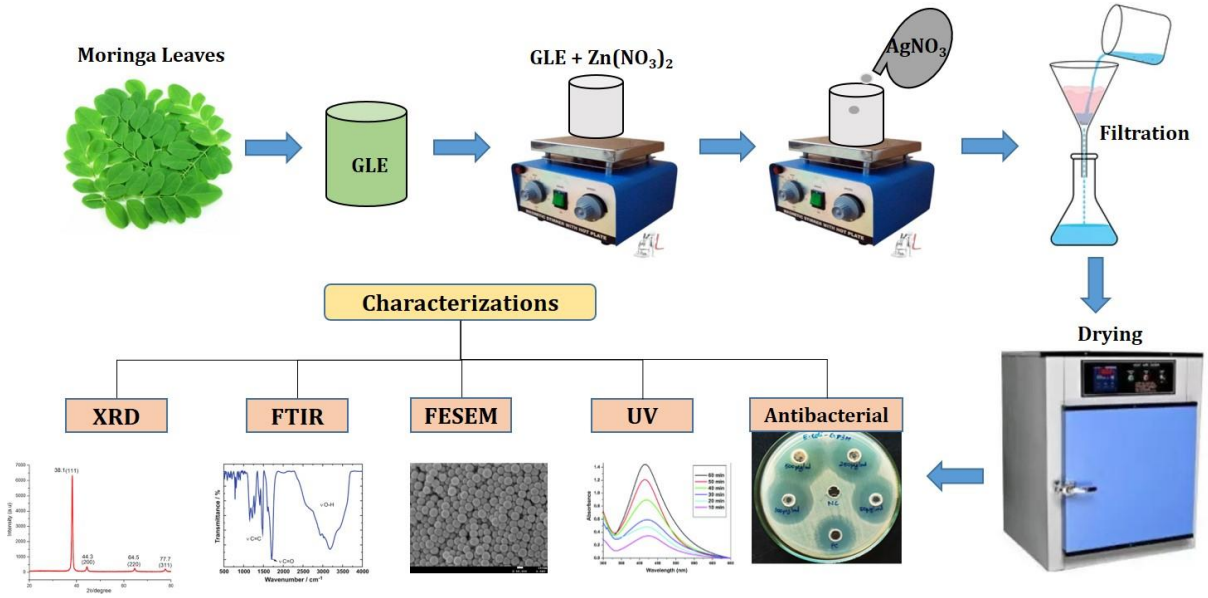

Fig. 1. Schematic representation of Ag/ZnO biosynthesis using Moringa leaf extract and characterization techniques

2. 3. Characterization

Powder diffraction data of Ag/ZnO nanocomposite was recorded with Bruker Eco D8 Advance X-ray diffractometer. Morphological analysis of Ag/ZnO nanocomposite was performed with ZEISS EVO 18 Model. The infrared (IR) spectra were obtained within the 4000-500 cm−1 range using a IR Tracer-100, SHIMADZU spectrophotometer. Additionally, the ultraviolet-visible (UV-Vis) spectrum was recorded using a JASCO-V770 UV-Vis-NIR spectrophotometer.

2. 4. Antibacterial Assay

The antimicrobial efficacy of the synthesized Ag/ZnO nanocomposites was evaluated against both gram-positive (Staphylococcus aureus - 902) and gram-negative (Escherichia coli

- 443) bacterial strains through the Agar well diffusion method. Petri plates containing 20 ml of nutrient agar medium were inoculated with a 24-hour culture of bacterial strains adjusted to a 0.5 OD value following the McFarland standard. Wells were then cut, and varying concentrations of the sample (500, 250, 100, and 50 µg/ml) were introduced. The plates were subsequently incubated at 37°C for 24 hours, and the antibacterial activity was assessed by measuring the diameter of the inhibition zone surrounding the wells. Gentamicin antibiotic served as a positive control, and the obtained values were calculated using Graph Pad Prism 6.0 software (USA).

3. RESULTS & DISCUSSION

3. 1. Structural Investigation of Pure Ag, ZnO and Ag/ZnO Nano-Composites

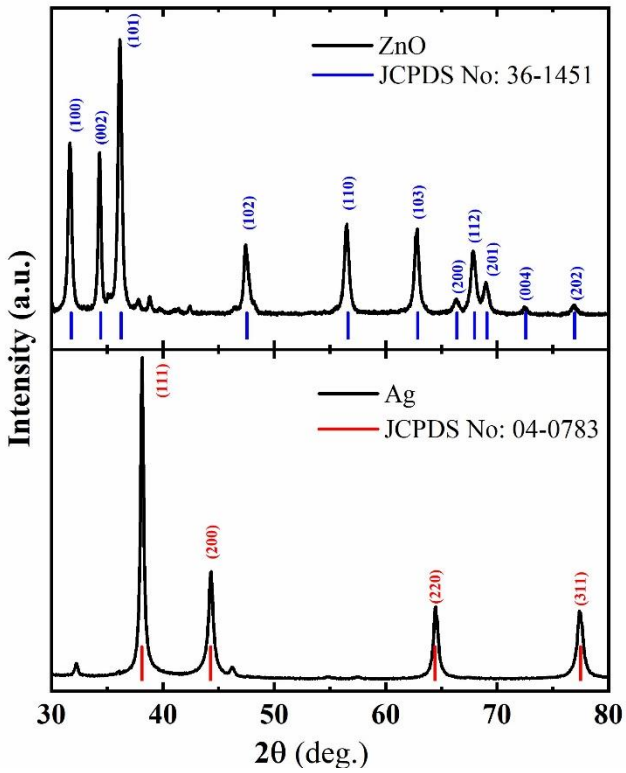

Fig. 2: Powder XRD pattern of pure ZnO (Top) and Ag (Bottom) nanoparticles synthesized using chemical method and compared with JCPDS card no: 36-1451 and 04-0783 respectively

Figure 2 presents the powder X-ray diffraction patterns of pristine ZnO (Top) and Ag (Bottom) nanoparticles synthesized via the co-precipitation method. The distinctive diffraction peaks corresponding to pure ZnO appear at 2θ values of 31.64°, 34.30°, 36.14°, 47.46°, 56.51°, 62.82°, 66.36°, 67.85°, 68.99°, 72.41°, and 76.96°. These peaks align with the crystal planes of (100), (002), (101), (102), (110), (103), (200), (112), (201), (004), and (202) in the hexagonal wurtzite structure of ZnO nanoparticles, in accordance with JCPDS file no. 36-1451, as denoted by vertical bars in Fig. 1 (Top) [23]. Similarly, distinct diffraction peaks of pure Ag emerge at 2θ values of 38.13°, 44.30°, 64.49°, and 77.44°, corresponding to the crystal planes of (111), (200), (220), and (311), respectively, in the Face-Centered Cubic structure. This alignment is consistent with JCPDS file no. 04-0783, as indicated by vertical bars in Fig. 2 (Bottom) [24]. The average crystallite size, calculated using Scherer's Equation, is determined to be 16 nm for pure ZnO and 13 nm for Ag respectively.

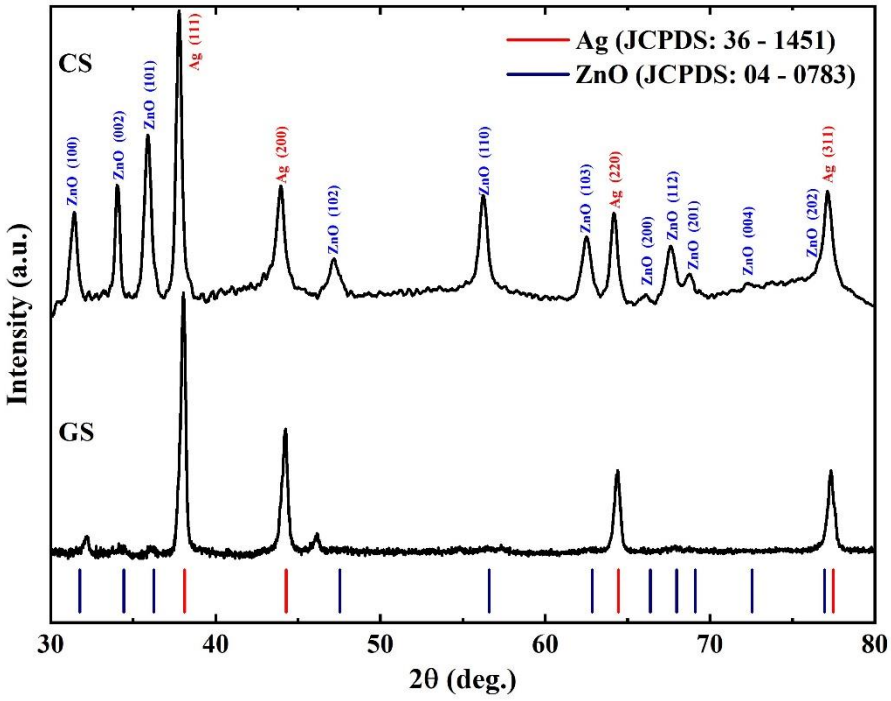

Fig. 3: Powder XRD patterns of Ag/ZnO nanocomposites synthesized through (Top) chemical (CS) and (Bottom) green synthesis (GS) methods

The X-ray diffraction (XRD) patterns of the Ag/ZnO nanocomposites synthesized through co-precipitation and green synthesis method using Moringa Oleifera as shown in Fig. 3, revealed distinctive peaks at specific 2θ values, indicating the crystallographic nature of both the samples. The obtained peak positons in both CS and GS samples confirm the hexagonal wurtzite structure of Zinc Oxide (ZnO) and Face-Centered Cubic structure of Silver, as evidenced by a strong match with JCPDS Card No. 36- 1451 and 04-0783 respectively. The simultaneous presence of ZnO and Ag phases confirms the successful formation of Ag/ZnO nanocomposites. The distinct peaks associated with each phase indicate that the crystalline integrity of the individual components has been retained during the synthesis process. Notably, the Ag peaks exhibit higher intensities, indicating a predominant presence of silver in the composite structure in both CS and GS samples.

3. 2 FT-IR Analysis of Ag/ZnO Nano-Composites

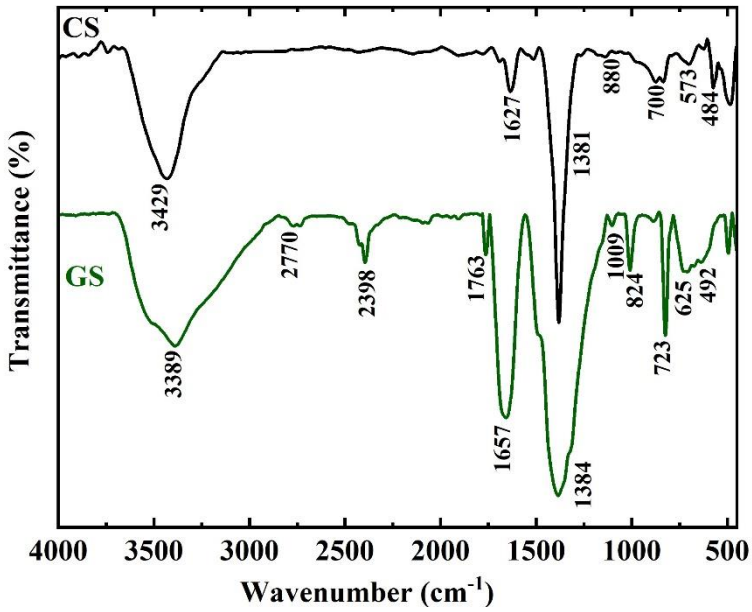

Fig. 4: FT-IR spectra of CS and GS samples

The FT-IR analysis of Moringa leaf extract provides valuable insights into its inherent composition as shown in Fig. 4. Both chemically synthesized (CS) and green-synthesized (GS) nanocomposites exhibit characteristic vibrational signatures. In both cases, the stretching and bending modes of ZnO occur in the ranges of 400-500 cm^{-1} and 300-600 cm^{-1}, respectively [15]. The vibrational modes associated with Ag-O bonding are present in the range of 500-700 cm^{-1}. However, the green synthesis method introduces unique features, such as strong asymmetric C-H stretching at 2398 and 2770 cm^{-1} in Moringa Oleifera, indicating the presence of organic ligands [25]. Additionally, the green-synthesized sample displays distinctive peaks, including asymmetric C-H bending at 1384 cm^{-1}, C-O stretching at 1009 cm^{-1}, and a robust amide band at 1657 cm^{-1}, suggesting the presence of carbohydrates and proteins. Hydroxyl groups contribute O-H stretching modes (3000-3600 cm^{-1}) in both chemically synthesized (CS) and green-synthesized (GS) nanocomposites [26]. This comparative analysis highlights the complementary information provided by FTIR spectroscopy in discerning molecular structures in chemically and green-synthesized nanocomposites.

3. 3 Morphology of Ag/ZnO Nano-Composites

The Field Emission Scanning Electron Microscopy (FESEM) images of the Ag/ZnO nanocomposite, synthesized via the co-precipitation method (CS), depict a distinctive flower-like morphology with intricate details, as shown in Fig. 5 (Top). In contrast, the green-synthesized (GS) samples (Fig. 5 (Bottom)) exhibit an almost rectangular shape. The average particle sizes, as determined through FESEM analysis, are approximately 22 nm for CS samples and 146 nm for GS samples. These observed morphologies suggest a unique self-assembly and growth pattern of the Ag/ZnO nanocomposite, influenced by factors such as the nature of the precursors, reaction conditions, and the presence of nucleation sites [27].

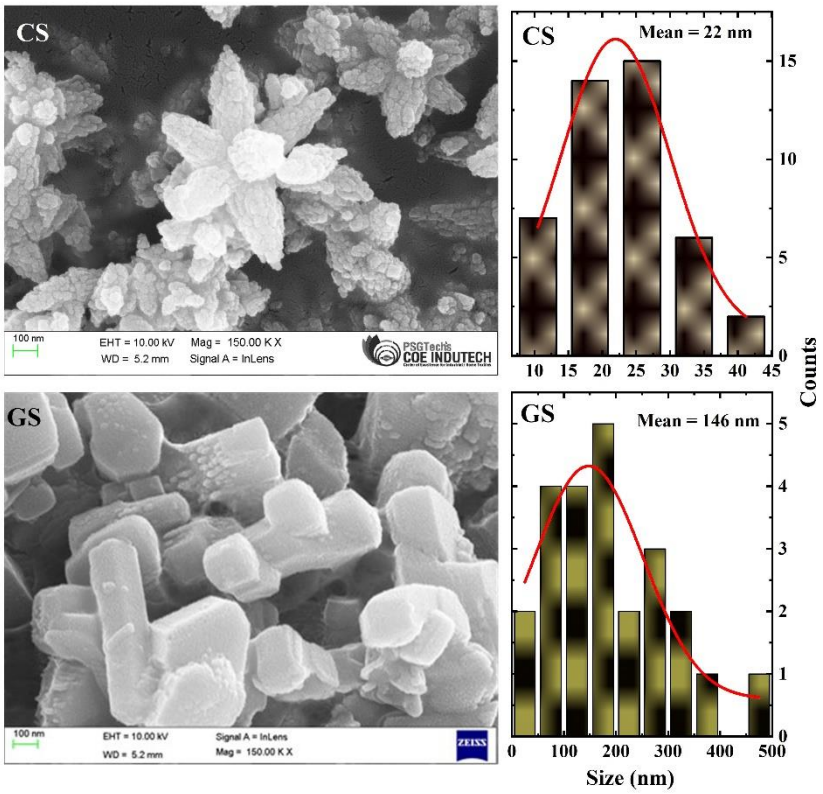

Fig. 5: FESEM morphological image of Ag/ZnO nanocomposite synthesized using co-precipitation method (Top) and green synthesis (Bottom)

3. 4 UV-Vis-NIR Spectroscopy Analysis

The optical band gap of Ag/ZnO nanocomposites, synthesized through co-precipitation and green synthesis methods, was assessed by analysing UV-Vis spectra within the 200-800 nm range, as depicted in Fig. 6. The peak absorption wavelength, observed around 300-330 nm in both samples (Fig. 6 a & b), corresponds to the energy needed for electron excitation in Ag/ZnO nanocomposites, aligning with previous findings [28]. In contrast to the visible range, the UV spectra of Ag/ZnO nanocomposites revealed peak absorption within the UV range, indicating a higher energy requirement for electron transitions between energy states. The

determination of the optical band gap utilized the Tauc plot method (Fig. 6 c & d), where absorbance was plotted against the corresponding wavelength (λ). This analysis yielded estimated values of direct band gaps, measuring at 3.12 and 3.1 eV for CS and GS samples, respectively. These values represent the minimum energy required for electrons to transition from the valence band to the conduction band in the material [29].

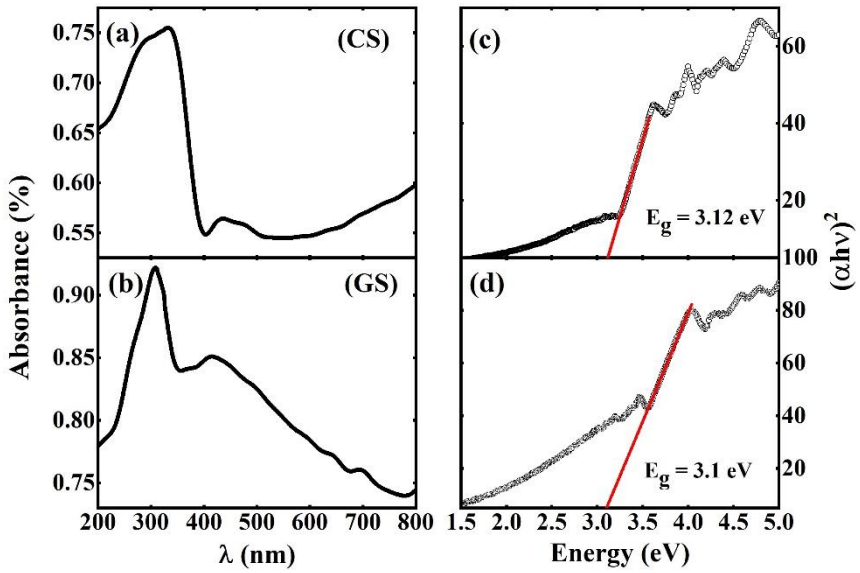

Fig. 6: UV-Vis absorbance spectra and Tauc plots of Ag/ZnO nanocomposite synthesized using co-precipitation and green synthesis method

3. 5 Antibacterial activities of Ag/ZnO nano-composites

The antibacterial efficacy of Ag/ZnO nanocomposites was investigated against both gram-positive (Staphylococcus aureus - 902) and gram-negative (Escherichia coli - 443) bacteria [30, 31] for both co-precipitation (CS) and green synthesis (GS) samples, as illustrated in Fig. 7 (a-d). In Fig. 6 (e & f), the inhibition zones of gram-negative and gram-positive bacteria for different concentrations of Ag/ZnO nanocomposites synthesized through chemical and green routes are presented. Surprisingly, in the negative control (Fig. 7 (e)), the CS sample exhibited no antibacterial activity. In contrast, the green-synthesized Ag/ZnO nanocomposite

demonstrated significant inhibition against Escherichia coli. Similarly, for the positive control, the growth inhibition efficiency of the GS sample surpassed that of the CS sample, as depicted in Fig. 7 (f). The robust antibacterial efficiency observed in the GS sample suggests its potential for further exploration in developing effective antibiotics against bacterial infections using Moringa Oleifera.

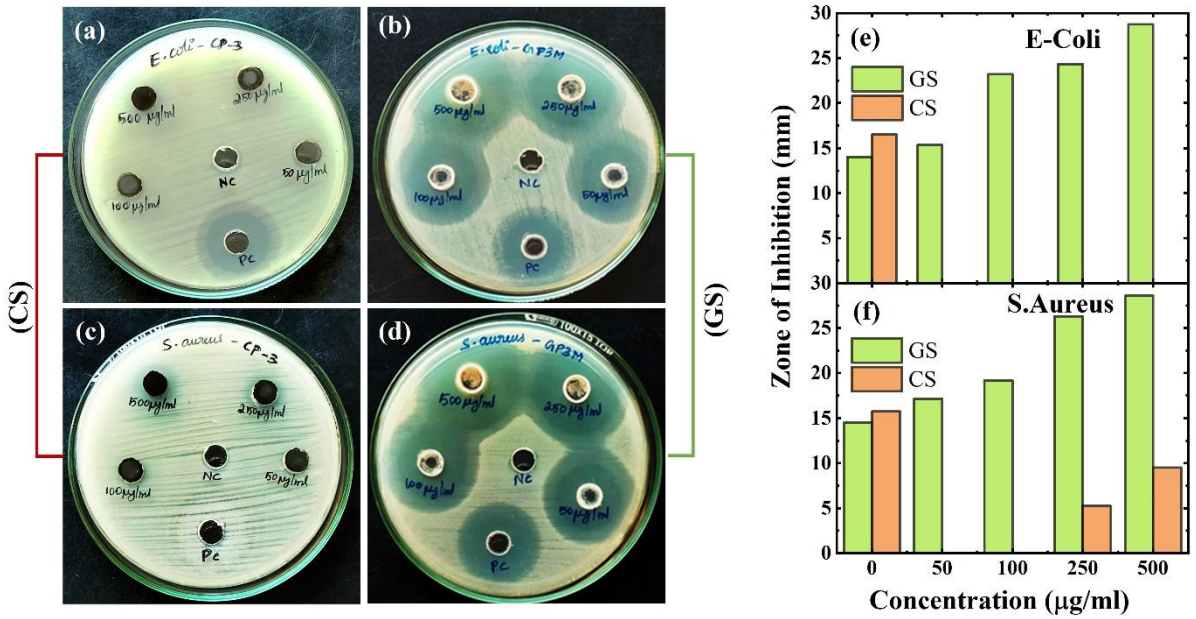

Fig. 7: (a-d) Antibacterial activity and (e & f) zone of inhibition of Ag/ZnO nanocomposites synthesized using co-precipitation (CS) and green synthesis (GS) method with different concentrations against Escherichia coli and Staphylococcus

4. Conclusions

In summary, the study focused on synthesizing Ag/ZnO nanocomposites through co-precipitation (CS) and green synthesis (GS) methods mediated by Moringa Oleifera and comprehensively characterized their structural, morphological, optical, and antibacterial properties. X-ray diffraction (XRD) patterns confirmed the hexagonal wurtzite structure of ZnO and Face-Centered Cubic structure of Ag in both samples, indicating the successful

formation of Ag/ZnO nanocomposites. FT-IR analysis highlighted distinctive vibrational signatures in both samples, with GS introducing unique features, suggesting the presence of organic ligands and biomolecules from Moringa Oleifera. Field Emission Scanning Electron Microscopy (FESEM) images revealed distinctive flower-like morphologies in CS samples and almost rectangular shapes in GS samples, showcasing unique self-assembly patterns influenced by synthesis conditions. UV-Vis spectra and Tauc plot analysis estimated direct band gaps of 3.12 eV for CS and 3.1 eV for GS samples. Antibacterial investigations demonstrated potent inhibition of both gram-positive and gram-negative bacteria, with the GS sample exhibiting superior efficacy, particularly against Escherichia coli. Ag/ZnO nanocomposites offer a unique combination of enhanced antibacterial properties, improved catalytic activity, and tunable electrical and optical characteristics. The synergy between silver and zinc oxide nanoparticles makes these nanocomposites valuable for applications in biomedicine, environmental remediation, and optoelectronics. This study underscores the potential of green-synthesized Ag/ZnO nanocomposites for developing efficient antibiotics against bacterial infections, leveraging the benefits of Moringa Oleifera-mediated green synthesis.

Acknowledgements

The Author, S. Magara Jothi Lakshmi acknowledges Nano Lab, Department of Physics, Sri Sarada College for Women (An Autonomous Institution), Tirunelveli - 627 011 for providing experimental facilities.

Authors' Contributions

SMJL: Conceptualization, methodology, formal analysis, investigation, writing original draft, visualization. **SGR**: conceptualization, writing-review and editing, supervision

References

1. Behzad F, Naghib SM, Tabatabaei SN, Zare Y, Rhee KY. An overview of the plant-mediated green synthesis of noble metal nanoparticles for antibacterial applications. Journal of Industrial and Engineering Chemistry. 2021;94:92-104.
2. Ahmed S, Kaur G, Sharma P, Singh S, Ikram S. Fruit waste (peel) as bio-reductant to synthesize silver nanoparticles with antimicrobial, antioxidant and cytotoxic activities. Journal of Applied Biomedicine. 2018; 16(3):221-31.
3. Mehata MS. Green route synthesis of silver nanoparticles using plants/ginger extracts with enhanced surface plasmon resonance and degradation of textile dye. Materials Science and Engineering: B. 2021; 273:115418.
4. Dimapilis EA, Hsu CS, Mendoza RM, Lu MC. Zinc oxide nanoparticles for water disinfection. Sustainable Environment Research. 2018; 28(2):47-56.
5. Matai I, Sachdev A, Dubey P, Kumar SU, Bhushan B, Gopinath P. Antibacterial activity and mechanism of Ag–ZnO nanocomposite on S. aureus and GFP-expressing antibiotic resistant E. coli. Colloids and Surfaces B: Biointerfaces. 2014; 115:359-67.
6. Irshad K, Khan MT, Murtaza A. Synthesis and characterization of transition-metals-doped ZnO nanoparticles by sol-gel auto-combustion method. Physica B: condensed matter. 2018; 543:1-6.
7. Asjadi F, Yaghoobi M. Characterization and dye removal capacity of green hydrothermal synthesized ZnO nanoparticles. Ceramics International. 2022; 48(18):27027-38.
8. Raj KP, Sadayandi K. Effect of temperature on structural, optical and photoluminescence studies on ZnO nanoparticles synthesized by the standard co-precipitation method. Physica B: Condensed Matter. 2016; 487:1-7.
9. Sharma DK, Shukla S, Sharma KK, Kumar V. A review on ZnO: Fundamental properties and applications. Materials Today: Proceedings. 2022; 49:3028-35.

10. Saha R, Karthik S, Balu KS, Suriyaprabha R, Siva P, Rajendran V. Influence of the various synthesis methods on the ZnO nanoparticles property made using the bark extract of Terminalia arjuna. Materials Chemistry and Physics. 2018; 209: 208-16.
11. Mohan S, Vellakkat M, Aravind A, Reka U. Hydrothermal synthesis and characterization of Zinc Oxide nanoparticles of various shapes under different reaction conditions. Nano Express. 2020; 1(3): 030028.
12. Karthikeyan M, Jafar Ahamed A, Karthikeyan C, Vijaya Kumar P. Enhancement of antibacterial and anticancer properties of pure and REM doped ZnO nanoparticles synthesized using Gymnema sylvestre leaves extract. SN Applied Sciences. 2019; 1: 1-9.
13. Condello M, De Berardis B, Ammendolia MG, Barone F, Condello G, Degan P, Meschini S. ZnO nanoparticle tracking from uptake to genotoxic damage in human colon carcinoma cells. Toxicology in Vitro. 2016; 35: 169-79.
14. Motshekga SC, Ray SS, Onyango MS, Momba MN. Microwave-assisted synthesis, characterization and antibacterial activity of Ag/ZnO nanoparticles supported bentonite clay. Journal of hazardous materials. 2013; 262:439-46.
15. Sharipova A, Slesarenko V, Gutmanas E. Synthesis of metal-metal oxide (Me-MenOm) nanocomposites by partial reduction and cold sintering. Materials Letters. 2020; 276:128197.
16. Panchal P, Paul DR, Sharma A, Choudhary P, Meena P, Nehra SP. Biogenic mediated Ag/ZnO nanocomposites for photocatalytic and antibacterial activities towards disinfection of water. Journal of colloid and interface science. 2020; 563:370-80.
17. Farooq, M., Shujah, S., Tahir, K., Nazir, S., Khan, A.U., Almarhoon, Z.M., Jevtovic, V., Al-Shehri, H.S., Hussain, S.T. and Ullah, A., Ultra efficient 4-Nitrophenol reduction, dye degradation and Cr (VI) adsorption in the presence of phytochemical

synthesized Ag/ZnO nanocomposite: A view towards sustainable chemistry. Inorganic Chemistry Communications, 2022; 136:109189.

18. Lam SM, Quek JA, Sin JC. Mechanistic investigation of visible light responsive Ag/ZnO micro/nanoflowers for enhanced photocatalytic performance and antibacterial activity. Journal of Photochemistry and Photobiology A: Chemistry. 2018; 353:171-84.
19. Mukunthan KS, Balaji S. Cashew apple juice (Anacardium occidentale L.) speeds up the synthesis of silver nanoparticles. International Journal of Green Nanotechnology. 2012; 4(2):71-9.
20. Bhalla N, Ingle N, Patri SV, Haranath D. Phytochemical analysis of Moringa oleifera leaves extracts by GC-MS and free radical scavenging potency for industrial applications. Saudi Journal of Biological Sciences. 2021; 28(12): 6915-28.
21. Belay K, Sisay MJ. Phytochemical constituents and physicochemical properties of medicinal plant (Moringa Oleifera) around bule hora. Chemistry and Materials Research. 2014; 6(7): 61-72.
22. Gopalakrishnan L, Doriya K, Kumar DS. Moringa oleifera: A review on nutritive importance and its medicinal application. Food science and human wellness. 2016; 5(2): 49-56.
23. Pavithra M, Raj MJ. Synthesis of ultrasonic assisted co-precipitated Ag/ZnO nanorods and their profound anti-liver cancer and antibacterial properties. Materials Science and Engineering: B. 2022; 278:115653.
24. Liu X, Du J, Shao Y, Zhao SF, Yao KF. One-pot preparation of nanoporous Ag-Cu@ Ag core-shell alloy with enhanced oxidative stability and robust antibacterial activity. Scientific reports. 2017; 7(1):10249.

25. Rauf MA, Zubair S, Ateeq H, Dabeer K, Pachauri S, Ajmal M, Owais M. Synergistic effect of diallyl sulfide with zinc oxide nanorods: a novel and effective approach for treatment of acute dermatitis in model animals. Frontiers in microbiology. 2018; 9:586.
26. Jing L, Xu Z, Sun X, Shang J, Cai W. The surface properties and photocatalytic activities of ZnO ultrafine particles. Applied Surface Science. 2001; 180(3-4):308-14.
27. Zeng X, Yang Z, Fan M, Cui F, Meng J, Chen H, Chen L. Shape-controlled growth of three-dimensional flower-like ZnO@ Ag composite and its outstanding electrochemical performance for Ni-Zn secondary batteries. Journal of colloid and interface science. 2020; 562:518-28.
28. Pandey PK, Chauhan V, Dixit P, Pandey PC. Correlation of enhanced photocurrent with structural and optical properties of Ag–ZnO nanocomposites synthesized by a facile chemical route. Physica B: Condensed Matter. 2021; 612:412937.
29. Guo Y, Fu X, Xie Y, Zhu L, Liu R, Liu L. Synthesis of Ag/ZnO nanocomposites with enhanced visible photocatalytic performance. Optical Materials. 2022; 133:112980.
30. Ibrahim HM. Green synthesis and characterization of silver nanoparticles using banana peel extract and their antimicrobial activity against representative microorganisms. Journal of radiation research and applied sciences. 2015; 8(3):265-75.
31. Ranjithkumar B, Kumar ER, Srinivas M, Ramalingam HB, Srinivas C, Magesh G, Balamurugan A, Rahale CS, ChandarShekar B. Evaluation of structural, surface morphological and thermal properties of Ag-doped ZnO nanoparticles for antimicrobial activities. Physica E: Low-dimensional Systems and Nanostructures. 2021; 133:114801.

Graphical Abstract

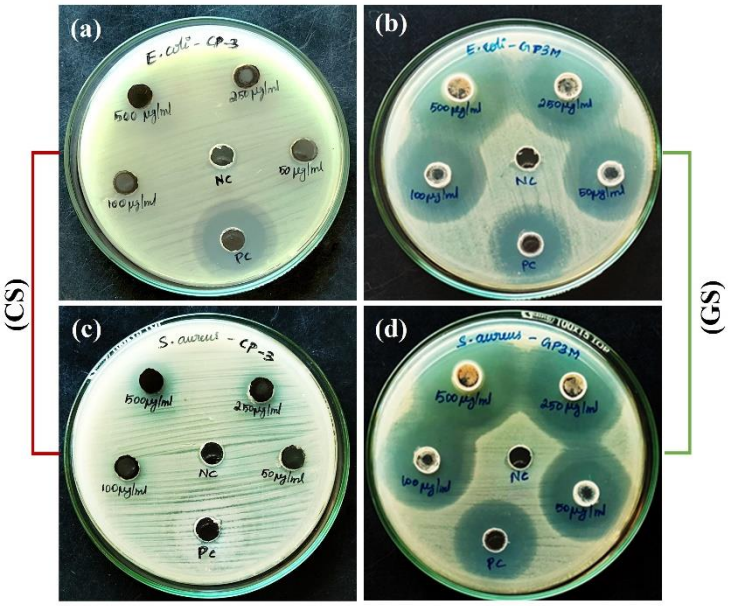
(a)
(b)
(c)
(d)
(CS)
(GS)
NC
PC

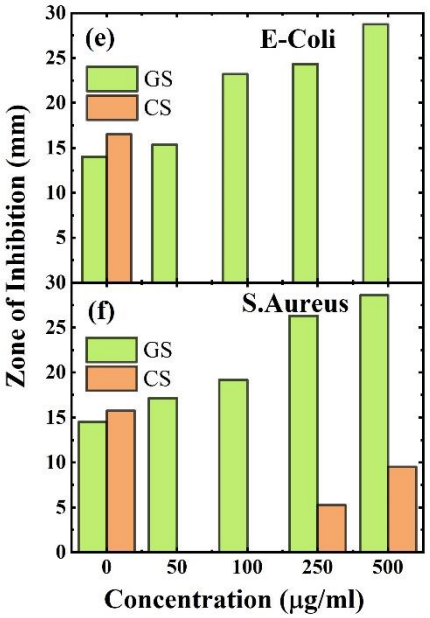
(e)
E-Coli
GS
CS
(f)
S.Aureus
Zone of Inhibition (mm)
Concentration (µg/ml)
0
50
100
250
500